Phase Fourier Reconstruction for Anomaly Detection on Metal Surface Using Salient Irregularity

Tzu-Yi Hung[1], Sriram Vaikundam[1], Vidhya Natarajan[1], and Liang-Tien Chia[2]

[1] Rolls-Royce@NTU Corporate Lab, Singapore,
[2] Nanyang Technological University, Singapore

Abstract. In this paper, we propose a Phase Fourier Reconstruction (PFR) approach for anomaly detection on metal surfaces using salient irregularities. To get salient irregularity with images captured from an automatic visual inspection (AVI) system using different lighting settings, we first trained a classifier for image selection as only dark images are utilized for anomaly detection. By doing so, surface details, part design, and boundaries between foreground/background become indistinct, but anomaly regions are highlighted because of diffuse reflection caused by rough surfaces. Then PFR is applied so that regular patterns and homogeneous regions are further de-emphasized, and simultaneously, anomaly areas are distinct and located. Different from existing phase-based methods which require substantial texture information, our PFR works on both textual and non-textual images. Unlike existing template matching methods which require prior knowledge of defect-free patterns, our PFR is an unsupervised approach which detects anomalies using a single image. Experimental results on anomaly detection clearly demonstrate the effectiveness of the proposed method which outperforms several well-designed methods [15], [8], [12], [18], [19], [16] with a running time of less than 0.01 seconds per image.

Keywords: anomaly detection, defect detection, saliency, unsupervised, automatic visual inspection, metal surface

1 Introduction

Automatic Visual Inspection (AVI) is one of the critical industrial applications which uses computer vision technology to assist human inspection in an effective and efficient manner. In such a system, anomaly detection is one of the challenging tasks with high demands [1], [2], [10]. For example, many issues have been discussed on electronic chips and integrated circuits for defect detection in images [7], [14], [4], [2].

In the literature, anomaly detection can be categorized into three types. The first type is to detect local textual irregularities on textured surfaces [1], [11], as an example shown in Fig. 1 (a). Many works on texture features and textural analysis have been discussed and investigated [17].

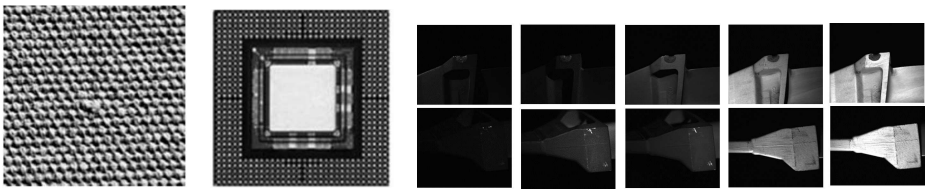

(a) (b) (c)

Fig. 1: Examples of different image sources. (a) a texture-based image [1], (b) an image with single lighting condition [2], and (c) an image set with multiple lighting conditions. Note that dark images at the left two columns are adjusted with 40% increase of brightness and contrast to be visible in the paper.

The second type is to detect abnormalities among defect-free examples, which is a typical application applied for die and chip inspections, as shown in Fig. 1 (b). Template matching is one of the traditional solutions discussed in this category [9], [2], [15], where anomalies are found by computing similarities between a test image and images in an anomaly-free set. In other words, prior knowledge such as a pre-collected template dataset is required.

The third type is to detect abnormalities using images of metallic components captured at pre-defined viewpoints and lighting conditions. Fig. 1 (c) shows two examples of how the changes in lighting directions influence the reflectivity of regions with and without anomalies on a metal surface. Note that dark images at the left two columns are adjusted to be visible in the paper. Between these two examples, the anomaly at the top row can be easily found in the bright images, but the one at the bottom is visually distinct in the dark images since it shines. Detection of such anomalies is a challenging task in a real-world application of AVI, but to our best knowledge, this area of research is yet to be explored.

In this paper, we are working on images from the third category for anomaly detection where not only different characteristics of anomalies are considered, but shapes of metallic objects are also taken into account which makes this task more challenging. Fig. 2 lists five examples of anomalies, which from left to right are melt, plus metal, scratch, scuff, and shadowing. Some of them are visually noticeable in bright images such as melt, plus metal and shadowing, but some of them shine in dark images such as scratch and scuff. Although certain anomalies may only be visually perceptible under certain lightings, we observed that because of diffuse reflection, those anomalies which are visually noticeable in bright images also appear irregularly salient in dark images when compared to its surroundings such as metal surface and shape boundary. Therefore, we propose to use PFR on dark images where details of smooth regions are reduced, but rough defect areas are highlighted. Our method outperforms several well-designed methods including saliency-based approaches, template matching, and keypoint detection schemes. Moreover, the processing time is less than 0.01 seconds per image, and no prior knowledge is required.

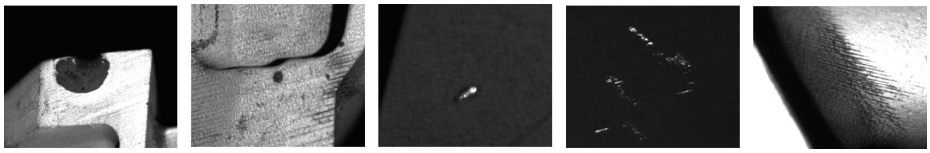

Fig. 2: Example of anomalies. From left to right are melt, plus metal, scratch, scuff and shadowing.

The rest of the paper is organized as follows. Section 2 introduces related work. Section 3 describes the proposed anomaly detection method. Section 4 shows the experimental results, and Section 5 concludes the paper.

2 Related Work

Most methods detect anomalies using images whose anomaly regions are clearly visible. Vaikundam *et. al.* [15] proposed to detect anomalies on a residue image which is obtained by a template matching approach. More specifically, they firstly performed a SIFT keypoint matching to find the best-match anomaly-free image compared to the given input and obtained a residue image between an anomaly-free image and an anomaly one. Then the SIFT keypoint detection method is applied again to detect regions of interest in the residue image. This method works well on those anomalies that are visually noticeable in bright images. However, it is hard to perform template matching using dark images since component shape and design, and foreground/background boundary are obscure. Moreover, template matching may be time-consuming which highly depends on the size of the template set.

On the other hand, Bai *et. al.* [2] proposed to use phase spectrum followed by a template matching method. Firstly, phase-only Fourier transform (POFT) is used to highlight potential anomalies on a collection of similar test images which is formed as an input matrix image for anomaly detection. Then a template matching step is adopted to finely compare local discrepancies between test images and anomaly-free templates, especially for those potential locations. This method needs several images to form a regular and repeated pattern when using POFT; otherwise, the method would fail for anomaly detection. Further, they only considered anomalies shown in the bright images. Instead, in our work, we apply PFR on a single dark image for anomaly detection without template matching.

Phase-based Fourier methods have been used for saliency detection and defect detection [6], [5], [1], [13], [3] such as automated surface inspection for directional textures [13], fabric defect detection [3], saliency detection on natural images[6] and videos [5], and texture-based surface defect detection [1]. The main difference is that they applied phase-based Fourier methods on bright images and tried to make input images into patterns.

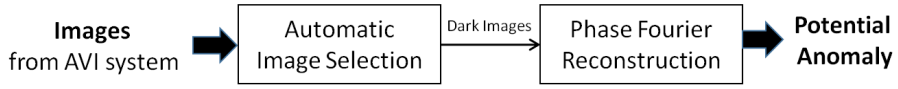

Fig. 3: Framework of the proposed anomaly detection method.

3 Anomaly Detection on Metal Surface

In this paper, we propose an anomaly detection method for AVI using PFR. Fig. 3 shows the framework. We firstly apply image selection to automatically select dark images as input to PFR for anomaly detection. The following subsections describe details of the proposed method.

3.1 Salient Irregularities in Dark Images

Most existing methods for anomaly detection aim to detect their targets using clearly visible images as mentioned earlier. Instead, we focus on salient irregularities in dark images. The key idea is the majority of image pixels on the metal surface are dark in such images, in particular for those smooth and homogenous areas; therefore the details of the surface become uniformly indistinct caused by specular reflection. On the other hand, irregular or abnormal regions become salient because of diffuse reflection on uneven surfaces. Fig. 4 shows an illustration of specular and diffuse reflections, respectively. In dark images, the diffuse reflection makes anomaly salient comparing to its smooth surrounding metal surface. For example, in Fig. 5 (a), a melt anomaly can be seen clearly in addition to details of the surface, shape of the component, and boundaries of the foreground and background, etc. Although the melt anomaly is visually salient, it is challenging to be detected as other details are also evident, in particular for regions of focus. On the contrary, in Fig. 5 (b), it is too dark to see every detail except for salient irregularities from the rough surface caused by the diffuse reflection. This diffusion effect emphasizes anomaly regions while eliminating object details. Therefore, in this paper, we aim at detecting different anomalies such as melt, plus metal, scratch and scuff using dark images based on their salient irregularities.

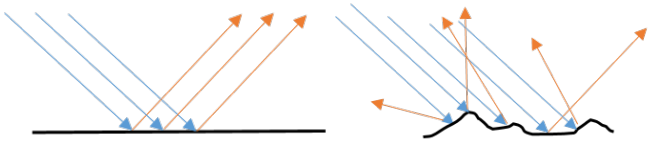

(a) Specular Reflection (b) Diffuse Reflection

Fig. 4: Example of reflections. (a) Specular reflection on smooth surface, and (b) diffuse reflection on rough surface.

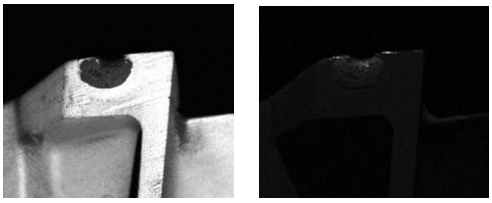

(a) Bright image (b) Dark image

Fig. 5: Example of an anomaly under different lighting conditions.

3.2 Automatic Image Selection

To get such dark images, we manually labeled a small collection of images according to their lighting conditions and trained a classifier using support vector machine (SVM). There are two advantages to using this method for automatic image selection. First, this is a simple and intelligent method for selecting images. Second, it is easy to be applied to all test samples without considering their shape and the ratio of background and foreground. More specifically, a small subset of dark, gray and bright images are chosen for training. In our experiments, we use 220, 70 and 74 images, accordingly. Then a multi-class SVM model is used to learn a dark/gray/light classifier, and only dark image outputs are adopted for anomaly detection.

3.3 Phase Fourier Reconstruction (PFR)

Although shape and design of the component, and boundaries of foreground and background are still visible in the selected dark images, they are de-emphasized due to lower pixel intensities on these smooth surfaces. Instead, anomaly region is emphasized because of the diffuse reflection on rough surfaces, as shown in Fig 5 (b). In this section, we proposed to use PFR for anomaly detection in such dark images. The proposed PFR removes regular patterns and homogeneous regions, but highlights salient regions which may likely be an anomaly. After PFR, a 2D Gaussian filter and a thresholding method are applied to generate the corresponding saliency map. The key idea of the PFR is as follows. First, we transform an image from its spatial domain to the frequency domain represented by magnitude and phase using Fourier transform. Then, the image is reconstructed back to its spatial domain using phase with unity magnitude. Corresponding color information is removed from the image by setting the magnitude to unity, and distinct irregularities such as edge boundaries are highlighted due to the phase effect. More specifically, given an image f with size of $N \times M$, the two-dimensional discrete Fourier transform can be defined as follows:

$$F(u,v) = \sum_{x=0}^{N-1} \sum_{y=0}^{M-1} f(x,y) e^{-j2\pi(\frac{ux}{N} + \frac{vy}{M})} \tag{1}$$

where $f(x, y)$ is the pixel in the spatial domain, $F(u, v)$ is the point in the Fourier domain, and u and v are spatial frequencies in x and y directions, respectively. We can rewrite the equation to separate the real and imaginary parts:

$$F(u, v) = F_R(u, v) + jF_I(u, v) \tag{2}$$

where $F_R(u, v)$ is the real part of $F(u, v)$, and $F_I(u, v)$ is the imaginary part of F(u,v) in the complex domain. It can also be expressed in polar form in terms of magnitude and phase:

$$F(u, v) = |F(u, v)|e^{j\angle F(u,v)} \tag{3}$$

where $|F(u, v)|$ and $\angle F(u, v)$ are magnitude and phase, respectively, which can be calculated using $F_R(u, v)$ and $F_I(u, v)$ as below:

$$|F(u, v)| = \sqrt{F_R(u, v)^2 + F_I(u, v)^2} \tag{4}$$

$$\angle F(u, v) = \arctan \frac{F_I(u, v)}{F_R(u, v)} \tag{5}$$

The PFR can be performed by providing the inverse Fourier transform of $F(u, v)'$ using the following equation for image reconstruction:

$$F(u, v)' = e^{j\angle F(u,v)} \tag{6}$$

where the magnitude is set to one, $|F(u, v)| = 1$, and the original phase is retained. The reconstructed image is denoted by $f(x, y)'$. Then a 2D Gaussian filter is applied on the reconstructed image $f(x, y)'$ to get a smoother image $g(x, y)$ with reduced noise. The standard deviation of the Gaussian distribution is equal to 3 in the experiment. Finally, a thresholding method is used to get the saliency map s(x,y):

$$s(x, y) = \begin{cases} 255 & \text{if } g(x, y) \geq \mu + C\sigma \\ 0 & \text{otherwise} \end{cases} \tag{7}$$

where μ is the mean value of g(x,y), σ is the standard deviation of g(x,y) and C is a constant which is set to 6 in our experiment. This means that only the pixel whose intensity is much larger than its mean is picked as anomaly. We show the PFR method in Algorithm 1.

4 Experimental Results

In this section, we analyze and evaluate the proposed PFR method for anomaly detection. We compare our method with four well-designed saliency detection methods [12], [18], [19], [16], a keypoint detection approach [8], and a template matching method [15]. The data used for this experiment is a subset of the

Algorithm 1 Phase Fourier Reconstruction for Anomaly Detection

Require: Given a dark image f
Ensure: Saliency map s for anomaly detection
1: Fourier Transform. Get F(u,v) from f(x,y) using Eq. (1) and Eq. (3).
2: Remove Magnitude. Get F(u,v)' using Eq. (6).
3: Phase Reconstruction. Get f'(x,y) using inverse Fourier transform on F(u,v)'.
4: Smoothing. Get g(x,y) using 2D Gaussian filter on f(x,y)'.
5: Thresholding. Get s(x,y) from g(x,y) using Eq. (7).

actual data set which was acquired as a part of the Automated Visual Inspection process with about 18,600 images of metallic components captured at pre-defined viewpoints and lighting conditions.[1] Each image has a resolution of 2448 x 2050 pixels. All methods are applied to 13 pairs of bright and dark images obtained using a trained SVM classifier for image selection with different anomalies on metal surfaces. The visualization of the resulting saliency maps for these bright and dark images are shown in Fig. 6 and Fig. 7, respectively.

4.1 Comparison between Dark and Bright Images Using PFR

The detection results of the proposed PFR method applied to the bright images are shown in Fig 6 (b). When applying PFR on the bright images, PFR fails in several cases as the details of the components are also salient along with the anomalies. Hence, no prominent peaks can be found after statistical thresholding. On the contrary, PFR works well on dark images because we utilize salient irregularities caused by diffuse reflection so that the details on smooth metal surfaces become visually obscure. This pattern-like effect makes anomalies salient among those regularities, as shown in Fig 7 (b). Comparing these results to the ground truth in Fig 7 (a), it can be observed that the proposed PFR method detects all the anomalies successfully. It is worth mentioning that while all dark images are adjusted for visualization, some of the anomalies still cannot be seen clearly. In such cases, please refer to the corresponding images in Fig 6 (a).

4.2 Comparison with Saliency Detection Methods

In this section, we compare our results with four well-established methods for saliency detection. They are geodesic saliency (GS) [16], manifold ranking (MR) [18], saliency filter (SF) [12] and saliency optimization (SO) [19]. Results are shown in columns (c), (d), (e) and (f) of Fig. 6 and Fig. 7. Different from our application, these methods are designed for detecting saliency maps using visually distinct images. From the visualization, we can see that these saliency methods fail to work well in both bright and dark cases. Most of them separate foreground and background or detect regions in focus. This is because they use background/foreground information such as background connectivity [16], [19],

[1] Limited disclosure due to confidentiality reasons

Fig. 6: Saliency maps from different anomaly detection methods applying on bright images. (a) Bright images with bounding boxes indicating locations of anomalies, (b) results from the proposed PFR, (c) Geodesic Saliency (GS) [16], (d) Manifold Ranking (MR) [18], (e) Saliency Filter (SF) [12], (f) Saliency Optimization (SO) [19], (g) Keypoint Detection (KD) [8], and (h) Template Matching (TM) [15].

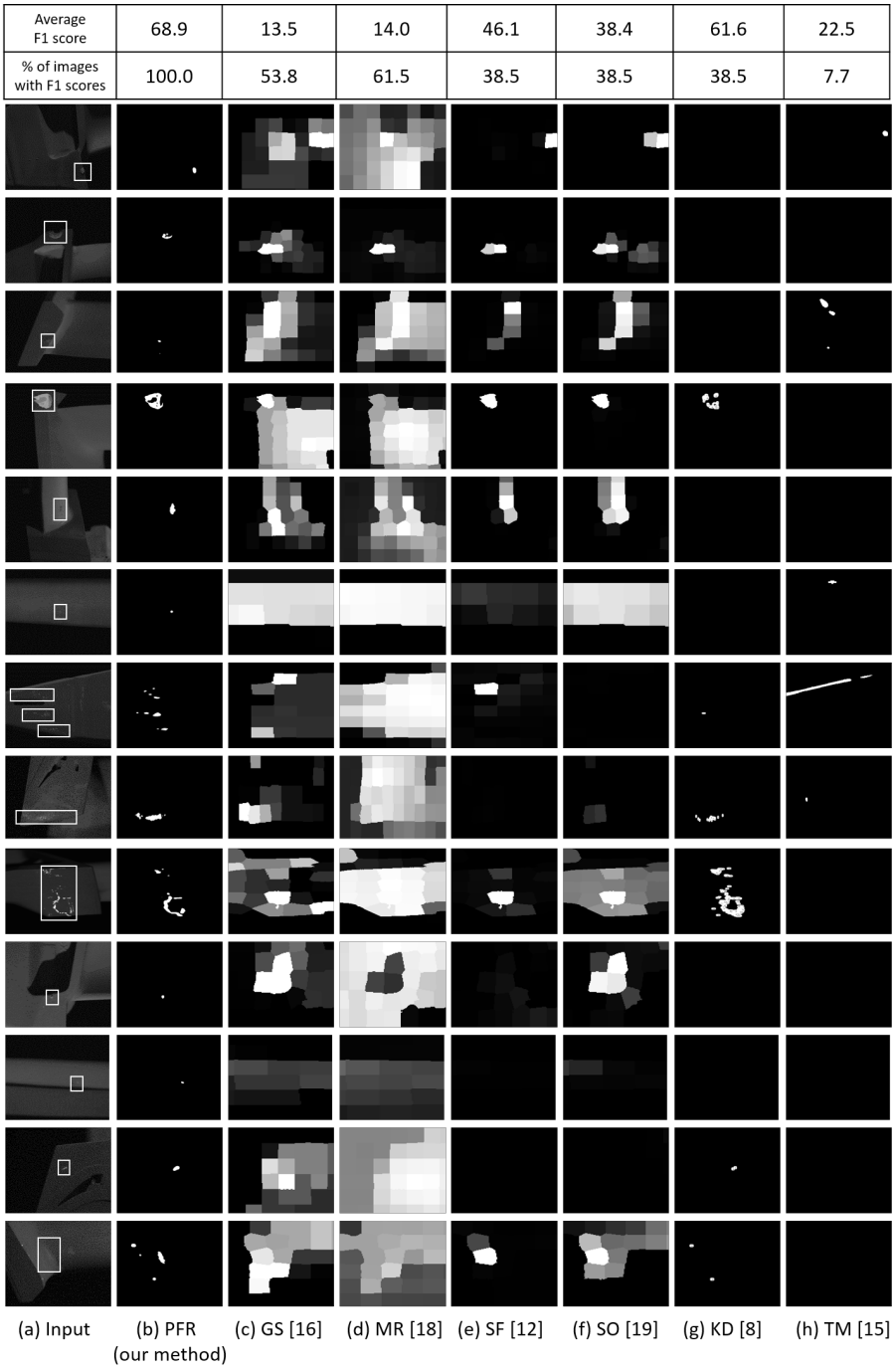

Fig. 7: Saliency maps from different anomaly detection methods applying on dark images. (a) Dark images with bounding boxes indicating locations of anomalies (images are adjusted for visualization), (b) results from the proposed PFR, (c) Geodesic Saliency (GS) [16], (d) Manifold Ranking (MR) [18], (e) Saliency Filter (SF) [12], (f) Saliency Optimization (SO) [19], (g) Keypoint Detection (KD) [8], and (h) Template Matching (TM) [15].

background and foreground cues [18] and contrast based filtering [12] to extract the saliency map of an image. On the other hand, in our images, we have a large portion of the component with silver metal surface and black background. Only a small region contains anomalies, so it is not surprising that these algorithms miss the anomaly regions although some of them are visually salient.

4.3 Comparison with a Keypoint Detection Method

In this section we compare our method with a popular keypoint detection (KD) method, SIFT [8], to evaluate the performance. Fig. 6 (g) and Fig. 7 (g) show the results using SIFT on the bright and dark images, respectively. SIFT keypoints perform well on those anomalies that shine in the dark images due to reflection; However, it cannot detect those irregularities which do not shine. On the other hand, when applying SIFT on the bright images, it detects those focus regions or component shapes instead of anomalies. Instead, the proposed PFR can detect most of the anomalies in the dark images well.

4.4 Comparison with a Template Matching Method

We compare our method with a template matching (TM) method [15] which is also designed for anomaly detection using images captured from AVI. Results are shown in both Fig. 6 (h) and Fig. 7 (h), respectively. We can see that the template matching method performs well on some of the bright images where those anomalies are visually salient. However, it fails to detect anomalies on dark images. The main reason is that finding the best-match template requires viewpoint matching which could be difficult to perform in the dark.

4.5 Evaluation

In this section, we calculate the F1 score to evaluate the performance of different methods. The equation of the F1 score is defined as follows:

$$F1 = 2 \times \frac{Precision \times Recall}{Precision + Recall} \tag{8}$$

where precision is the percentage of detected results that are correct and recall is the percentage of ground truth that is detected. The F1 score has a range from a worst score of 0 to a best score of 100. It should be noted that the F1 score is undefined when the Precision + Recall = 0 which occurs in images where only false alarms are detected, or when the Precision is undefined which occurs in images whose saliency maps are NULL without any detection. Hence, the average F1 score is computed using the sum of valid F1 scores dividing by the number of test images considered. Individual results are listed at the top of each corresponding column in Fig. 6 and Fig. 7, respectively. Fig. 8 shows four quadrants separating the average F1 score and the percentage of images considered into high and low regions for comparison. Only PFR applied on dark

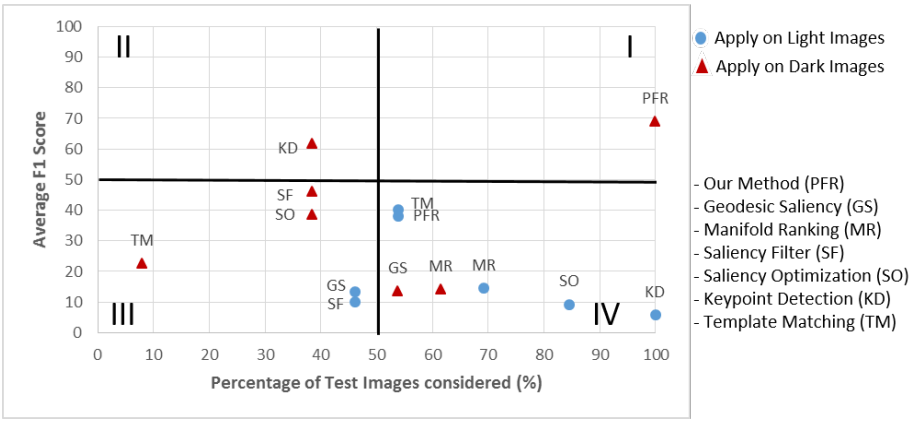

Fig. 8: Results between average F1 score and percentage of images with F1 scores from different approaches applying on bright and dark images

images can achieve a high F1 score with 100% of test images considered as shown in Quadrant I. Besides, the processing time per image is less than 0.01 seconds. While 40% of anomalies in the dark images are detected using Keypoint Detection (KD), as shown in Quadrant II, the remaining images are too dark to be detected. Although Salient Filter (SF) and Salient Optimization (SO) detect some anomalies on dark images similar to KD, their average F1 scores are lower and below 50% as shown in Quadrant III as they have more false alarms or missed detections. It is also worth mentioning that, Template Matching (TM) and PFR applied on bright images can detect some anomalies as well; however, similar to SF and SO, they also detect more false alarms or missed detections as shown in Quadrant IV.

5 Conclusion

In this paper, we have proposed a phase Fourier reconstruction method (PFR) for anomaly detection on metal surface which utilizes the characteristics of salient irregularities. Experiments on anomalies clearly demonstrate that our method outperforms the well-designed saliency detection methods, the template matching approach, and the keypoint detection method. We have shown the effectiveness and efficiency of the proposed method which is applicable for real industrial applications.

Acknowledgement This work was conducted within Rolls-Royce@NTU Corporate Lab with the support of National Research Foundation under the CorpLab@University scheme.

References

1. Aiger, D., Talbot, H.: The phase only transform for unsupervised surface defect detection. In: IEEE Conference on Computer Vision and Pattern Recognition (CVPR). pp. 295–302 (June 2010)
2. Bai, X., Fang, Y., Lin, W., Wang, L., Ju, B.F.: Saliency-based defect detection in industrial images by using phase spectrum. IEEE Transactions on Industrial Informatics 10(4), 2135–2145 (Nov 2014)
3. Chan, C.H., Pang, G.K.H.: Fabric defect detection by fourier analysis. IEEE Transactions on Industry Applications 36(5), 1267–1276 (Sept 2000)
4. Gao, H., Ding, C., Song, C., Mei, J.: Automated inspection of e-shaped magnetic core elements using k-tsl-center clustering and active shape models. IEEE Transactions on Industrial Informatics 9(3), 1782–1789 (Aug 2013)
5. Guo, C., Ma, Q., Zhang, L.: Spatio-temporal saliency detection using phase spectrum of quaternion fourier transform. In: IEEE Conference on Computer Vision and Pattern Recognition (CVPR) (June 2008)
6. Hou, X., Zhang, L.: Saliency detection: A spectral residual approach. In: IEEE Conference on Computer Vision and Pattern Recognition (CVPR) (June 2007)
7. Li, W.C., Tsai, D.M.: Defect inspection in low-contrast lcd images using hough transform-based nonstationary line detection. IEEE Transactions on Industrial Informatics 7(1), 136–147 (Feb 2011)
8. Lowe, D.G.: Distinctive image features from scale-invariant keypoints. International Journal of Computer Vision 60(2), 91–110 (2004)
9. Mattoccia, S., Tombari, F., Stefano, L.D.: Efficient template matching for multi-channel images. Pattern Recognition Letters 32(5), 694 – 700 (2011)
10. Neogi, N., Mohanta, D.K., Dutta, P.K.: Review of vision-based steel surface inspection systems. Journal on Image and Video Processing 2014(1), 1–19 (2014)
11. Ngan, H.Y., Pang, G.K., Yung, N.H.: Automated fabric defect detectiona review. Image and Vision Computing 29(7), 442 – 458 (2011)
12. Perazzi, F., Krhenbhl, P., Pritch, Y., Hornung, A.: Saliency filters: Contrast based filtering for salient region detection. In: IEEE Conference on Computer Vision and Pattern Recognition (CVPR). pp. 733–740 (June 2012)
13. Tsai, D.M., Hsieh, C.Y.: Automated surface inspection for directional textures. Image and Video Computing 18(1), 49–62 (1999)
14. Tsai, D.M., Wu, S.C., Chiu, W.Y.: Defect detection in solar modules using ica basis images. IEEE Transactions on Industrial Informatics 9(1), 122–131 (Feb 2013)
15. Vaikundam, S., Hung, T.Y., Chiat, L.T.: Anomaly region detection and localization in metal surface inspection. In: IEEE Conference on International Conference of Image Processing (ICIP) (Sept 2016)
16. Wei, Y., Wen, F., Zhu, W., Sun, J.: Geodesic saliency using background priors. In: European Conference on Computer Vision (ECCV). pp. 29–42 (2012)
17. Xie, X.: A review of recent advances in surface defect detection using texture analysis techniques. Electronic Letters on Computer Vision and Image Analysis 7(3), 1–22 (2008)
18. Yang, C., Zhang, L., Lu, H., Ruan, X., Yang, M.H.: Saliency detection via graph-based manifold ranking. In: IEEE Conference on Computer Vision and Pattern Recognition (CVPR). pp. 3166–3173 (June 2013)
19. Zhu, W., Liang, S., Wei, Y., Sun, J.: Saliency optimization from robust background detection. In: IEEE Conference on Computer Vision and Pattern Recognition (CVPR). pp. 2814–2821 (June 2014)